

PIV MEASUREMENTS ON A DELTA WING WITH PERIODIC BLOWING AND SUCTION

S. G. Siegel*, Thomas E. McLaughlin†, and Julie A. Morrow‡

*Department of Aeronautics
US Air Force Academy, CO 80840-6222*

Abstract

The mechanism by which periodic blowing and suction at the leading edge improves lift and stall angle of a 70° sweep delta wing is investigated in water tunnel experiments using PIV measurements. Periodic sinusoidal blowing and suction with zero net mass flux is applied at the leading edge of the wing. The experiments were conducted at a freestream flow speed of 0.126 m/s, corresponding to a root chord Reynolds number of 25,000. The wing was kept at an angle of attack of 35° for this study. A forcing frequency of $F^+ = 1.75$ was used, which was shown in previous research to be most effective in improving lift. The momentum coefficient was kept constant at (C_μ) of 0.004.

The two main vortices that dominate the unforced flow field are stationary without forcing. With forcing, however, the vortex centers travel both in spanwise and wing normal direction along an elliptic path. The streamwise vortex breakdown location is not changed as determined by measurements of the streamwise vorticity component. Instead, the forcing increases the axial velocity downstream of the vortex breakdown location, thus decreasing the local surface pressure and increasing normal force. This effect is attributed to the formation of a shear layer vortex during the blowing cycle, which carries high momentum fluid into the wake left downstream of the main vortex breakdown. The wake is weakened in synchronization with the presence of the shear layer vortex through the forcing cycle.

Nomenclature

B	Local wing span
C	Wing root chord
H	Forcing slot height, 1.5mm
C_μ	$=2(H/C)\langle u' \rangle / U_\infty^2$, Oscillatory momentum coefficient
f	Frequency
F^+	$(f \cdot C) / U_\infty$, nondimensional frequency
$\langle u' \rangle$	R.M.S. amplitude of velocity fluctuations
U_∞	Freestream velocity
X, Y, Z	Cartesian coordinates fixed with the wing. Origin at the wing apex, X axis is aligned with the root chord line.

U, V, W Velocity components of the flow in the X, Y, Z directions.

α Wing angle of attack

Introduction

The need to improve fighter aircraft and missile maneuverability has inspired extensive study of the flow past delta wings and of methods to delay vortex breakdown. In recent years, the efficacy of oscillatory flow excitation with zero net mass flux and non-zero momentum flux has been shown¹⁻⁹. It is more effective for delaying separation from a lifting surface or promoting reattachment of initially separated flow, relative to steady blowing traditionally used for this purpose. This concept has been proven for a delta wing¹⁻², some basic configurations^{4,5}, airfoils⁶ and a swept-back configuration⁷.

Guy et al¹ conducted a preliminary wind tunnel investigation and reported that periodic blowing and suction delays vortex breakdown and increases the local velocity over a delta wing after the onset of vortex breakdown. The increased velocity indicates a decrease of the local pressure; hence an increase of the lift force can be

* Postdoctoral Researcher, Department for Aeronautics, Member

† Research Associate, Department for Aeronautics, Senior Member

‡ Associate Professor Department for Aeronautics, Associate Fellow

This paper is declared a work of the U.S. Government and is not subject to copyright protection in the United States.

anticipated at angles of attack where vortex breakdown exists without flow excitation. Based on time averaged LDV velocity measurements and oil flow visualization, they concluded that periodic blowing and suction, applied at the leading edge of a delta wing, increases lift and delays vortex breakdown by approximately 0.35 chord length at 35° angle of attack.

Following these encouraging results, Guy et al² found that the periodic flow excitation delays wing stall and greatly increases the normal force at angles of attack where stall would have occurred otherwise. At a constant oscillatory momentum coefficient, the effect of the flow excitation is maximized at a non-dimensional frequency (F^+) of 1.75. At a constant frequency, an almost asymptotic increase of the normal force is observed as the momentum coefficient increases. The effect of the periodic flow excitation reaches its maximum at a momentum coefficient (C_m) of 0.004 approximately. These results are consistent with results that were obtained in previous investigations. A maximum increase of 38% in the normal force was obtained at an angle of attack of 40° at the test conditions, relative to the unforced case. A 10° delay of the stall angle was achieved.

Despite these encouraging results, the nature of the mechanism by which periodic blowing and suction couples to and interacts with the primary delta wing vortex has been elusive. Standard surface pressure, global force measurement and oil or smoke flow visualization have proven inadequate in illustrating how the oscillating velocity at the leading edge of the delta wing couples to and influences the primary vortex. This paper outlines the results of a particle image velocimetry (PIV) study at

the USAF Academy, wherein flow behavior on the suction side of a 70° delta wing is studied throughout the blowing/suction oscillation cycle. Through this effort, time histories of the velocity flow field illustrate flow behavior and the mechanism of lift increase in the presence of this type of flow control.

Experimental Setup

A flat-plate delta wing with a leading-edge sweep of 70° and a 25° bevel on the lower surface, was investigated in the USAF Academy 38 cm x 110 cm free-surface water tunnel. The wing has a chord length of 298 mm, is hollow and has a 1.5 mm wide slot along its leading edge. The wing was sting-mounted and placed inverted at an angle of attack of 35 degrees in the water tunnel.

To perturb the shear layer originating at the leading edge of the delta wing, a semi-spherical rubber cap was used as an oscillatory blowing and suction flow actuator. It was moved back and forth by a connecting rod, eccentrically mounted on a disk that was driven by a 560 W DC motor. The water displacement produced by the moving cap was channeled through a tube 2 cm in diameter to the hollow wing and to the length of the slot in its leading edge. The setup is depicted in Figure 1. With this setup, as with any oscillatory flow control method, fluid is drawn into the actuator over half of the sinusoidal cycle, and ejected over the other half ($V=V_0 \sin \omega t$). The phase during the forcing cycle is determined by the position of the rotating disk flywheel, which features an adjustable optical pickup to synchronize the data acquisition with a particular phase of the forcing cycle. A forcing cycle starts

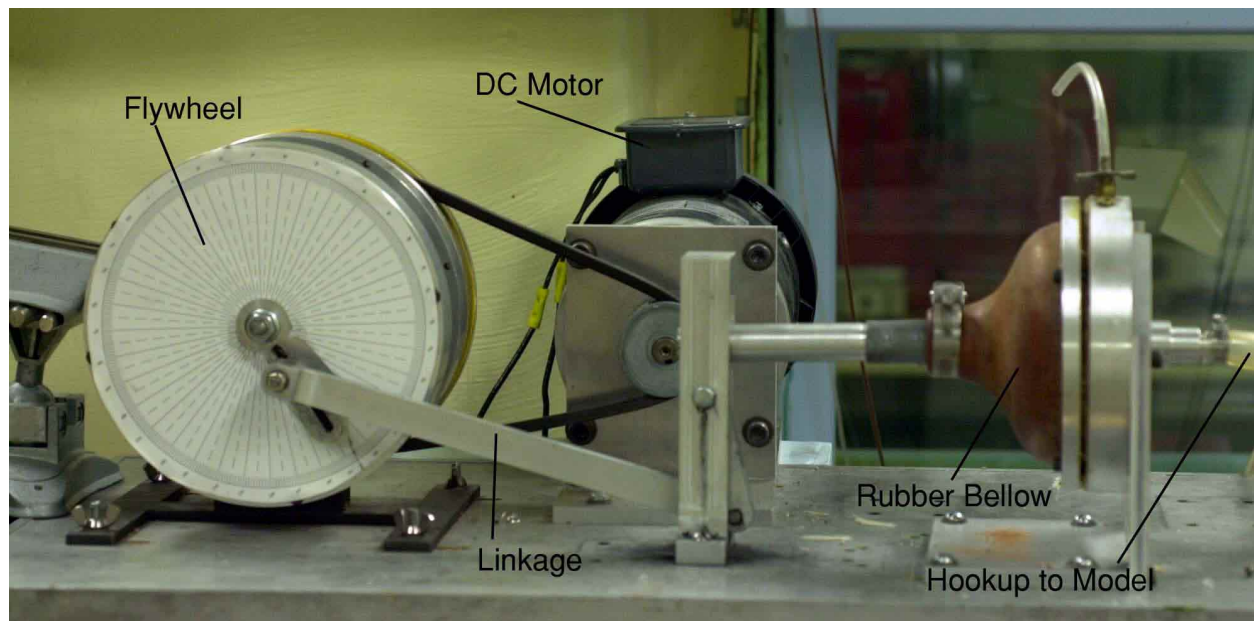
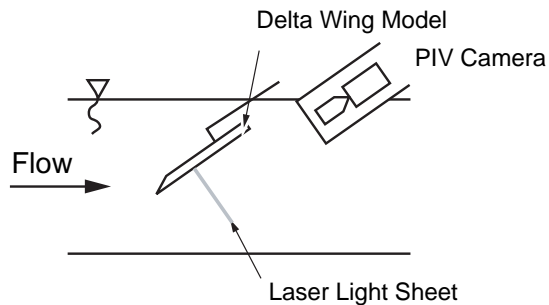


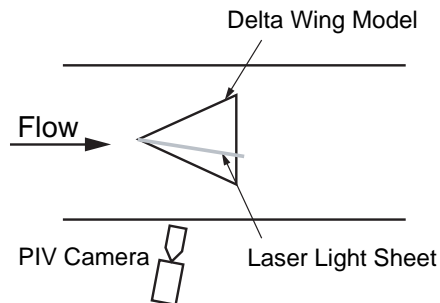
Figure 1 Oscillatory flow actuator.

Measurements across vortex core



Side View of Test Section

Measurements along vortex core



Top View of Test Section

Figure 2 PIV camera and model setup for measurements.

at 0° with the blowing phase which extends to 180° . The suction portion between 180° and 360° completes the cycle.

Measurement technique, data acquisition and post processing

To sample the flow, a Dantec Flowmap two-component PIV system with a New Wave Gemini 125 mJ Nd:Yag laser operating at 532 nm was used. A Kodak Megaplug ES 1.0 CCD camera (1000 x 1000 pixel resolution) was mounted downstream of the delta wing, to visualize the flow in a plane perpendicular to the model suction surface (Figure 2). A special plexiglass viewing box was used to facilitate viewing of planes perpendicular to the wing, avoiding the inherent refraction from the water surface. For measurements in a plane at a constant spanwise location, the laser was set up below the test section illuminating the flow from below, while the camera imaged the flow through the side window.

The operating parameters for the PIV system were kept constant throughout the study. Seeding was provided using $20\ \mu\text{m}$ Polyethylene particles. The system operated in cross correlation mode using two images, which were correlated in the frequency domain. Before correlation, a 3x3 Low pass filter was used to widen the particle images. A 32x32 pixel interrogation area was used, and the images were processed with 75 % overlap yielding a raw vector field of 123 x 123 vectors. The vector acceptance criteria were a peak ratio of at least 1.2, and 25% maximum velocity variation from neighboring vectors.

PIV images were phase-referenced to the forcing mechanism, to allow phase averaging of ten images, thus increasing signal-to-noise ratio of the data. Data sets were obtained every ten degrees through the 360° forcing cycle. Basic data reduction was done using the Flowmap

PIV software for vector validation, spatial moving average smoothing in a 3 x 3 vector area and averaging of the ten data sets. The data was then imported into LabVIEW-based post processing software for further data reduction and analysis. Plotting was done using TechPlot software by Amtec Inc.

Results and Discussion

Figure 3 shows the vorticity inherent in the unforced case. The figure shows the vorticity field at the 40% of root chord location, over approximately 25% of the local span, which extends from $2^*Y/B = -1$ to $2^*Y/B = 1$. As expected, the highest vorticity resides at the center of the primary delta wing vortex, located at $2^*Z/B = 0.37$ and $2^*Y/B = 0.62$. These values agree well with previous research at the Academy. A secondary vortex of opposite sign can be observed near the delta wing surface. At the tip of the wing a center of rotation exists that does not correlate with a peak in vorticity as can be seen from the closeup in Figure 3. In this closeup streamlines are shown to illustrate this effect.

The horizontal and vertical velocity profiles of the unforced flow are shown in Figure 4, at span distances and heights through the center of the vortex, as well as a horizontal profile at a height equal to 5% of the span, and a vertical velocity profile at the wing tip. Both spanwise (v) and wing normal (w) components of the velocity are shown. All profiles shown are measured at 40% chord. These profiles are consistent with the presence of the main vortex above the wing. The vertical component in the horizontal profile is consistent with the presence of the strong main vortex, as indicated by a sharp change in velocity as the vortex is traversed. Likewise, the horizontal component in the vertical profile exhibits the same behavior.

The flow near the surface is characterized as a

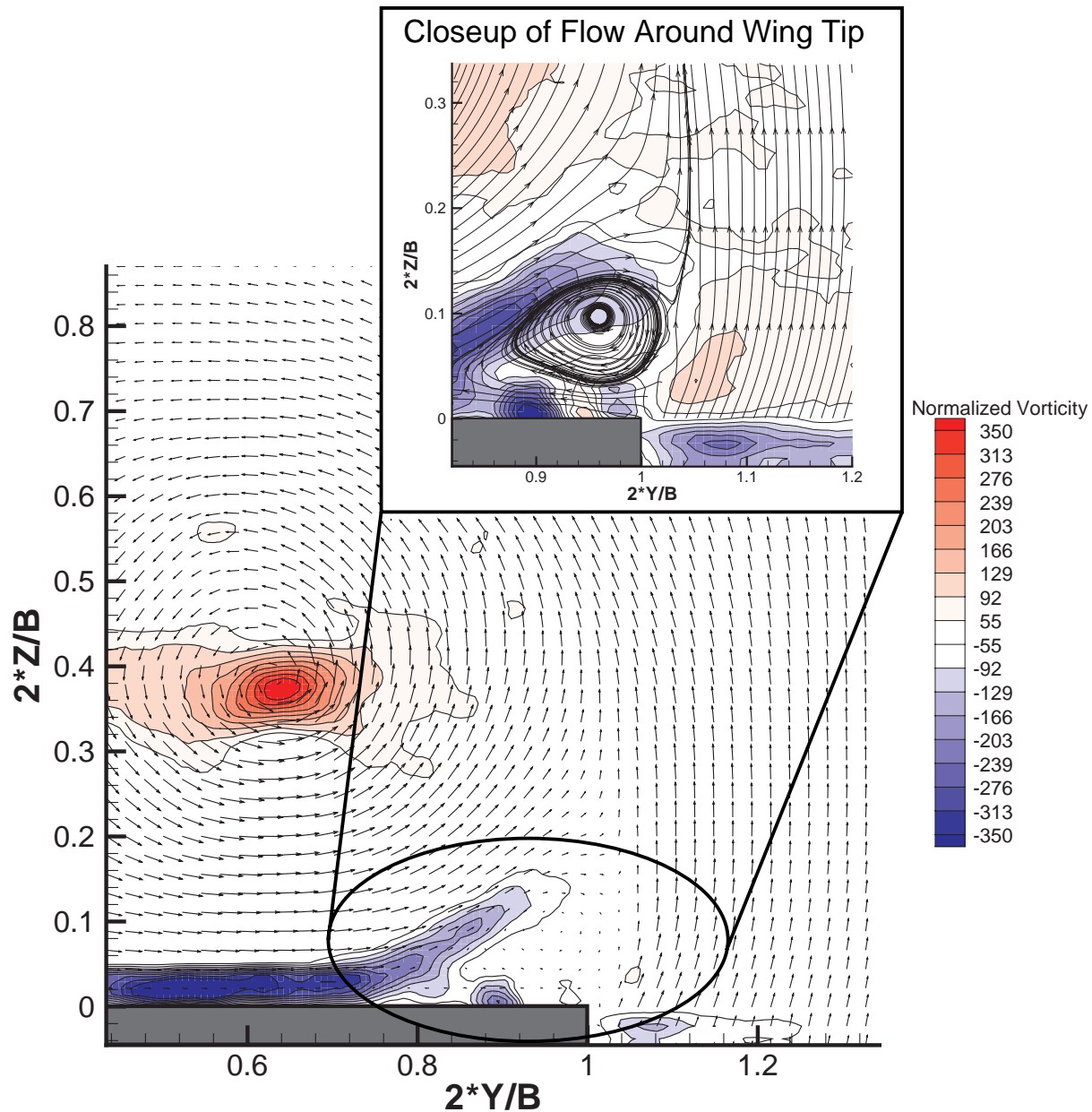


Figure 3 Average vorticity without forcing. $X/C = 0.4$, Field of view perpendicular to wing surface. Inset shows a closeup view of the flow around the wing tip, including streamlines.

relatively slow and constant vertical component across the wing, spiking upward at the tip due to the shear layer arising from the tip vortex. The spanwise component near the surface is highest directly below the primary vortex, indicative of flow induced by the vortex itself.

At the tip, the vertical component of velocity decreases, then increases as distance above the wing increases. It peaks at 0.5 span widths above the wing, consistent with the feeding vortex sheet crossing the wing tip plane. The spanwise component reaches a maximum just above the surface, then minimum at 0.5 span width. Both

are consistent with the direction of the feeding vortex sheet from the leading edge.

Figure 5 shows the fluctuation of the circulation in the shear layer and the main vortex through the forcing cycle. Circulation was calculated by integrating the vorticity field, after thresholding the vorticity at 10% of the peak value to remove background noise. The unforced case is shown for reference. It is clear that the circulation in the main and forcing vortices vary substantially over the course of the forcing cycle. The circulation in the main vortex reaches a minimum of about 50%, and a maxi-

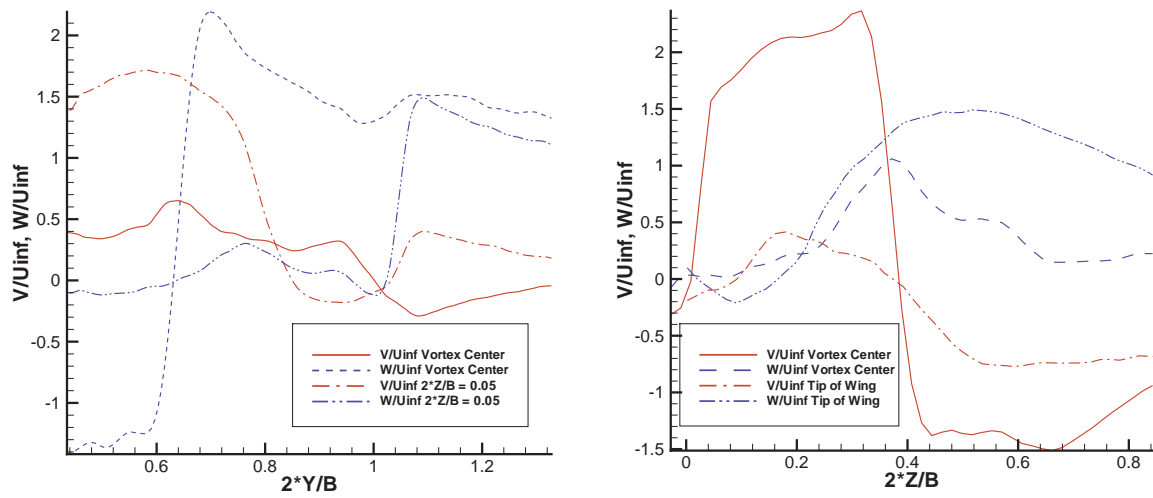


Figure 4 Horizontal and vertical velocity profiles, unforced flow, 40% chord.

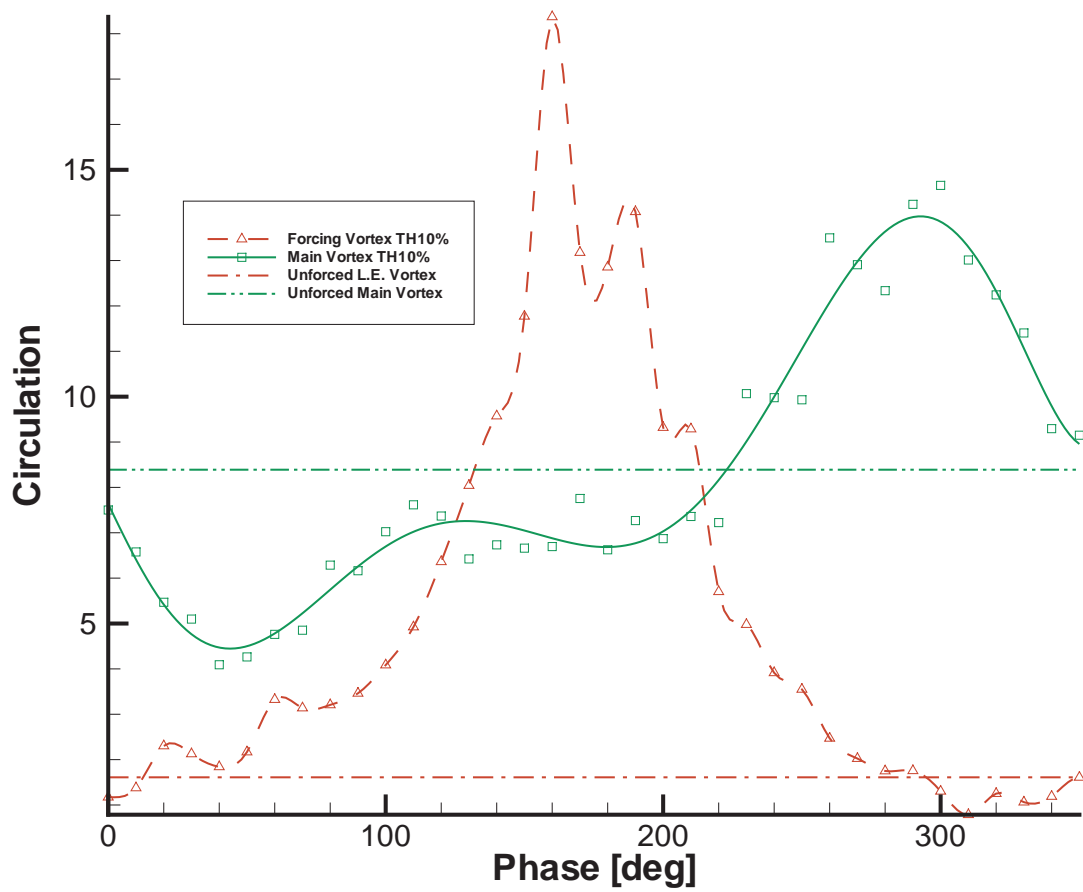


Figure 5 Circulation of main vortex and forced vortex, normalized with the free stream velocity and chord length. $F+ = 1.75$.

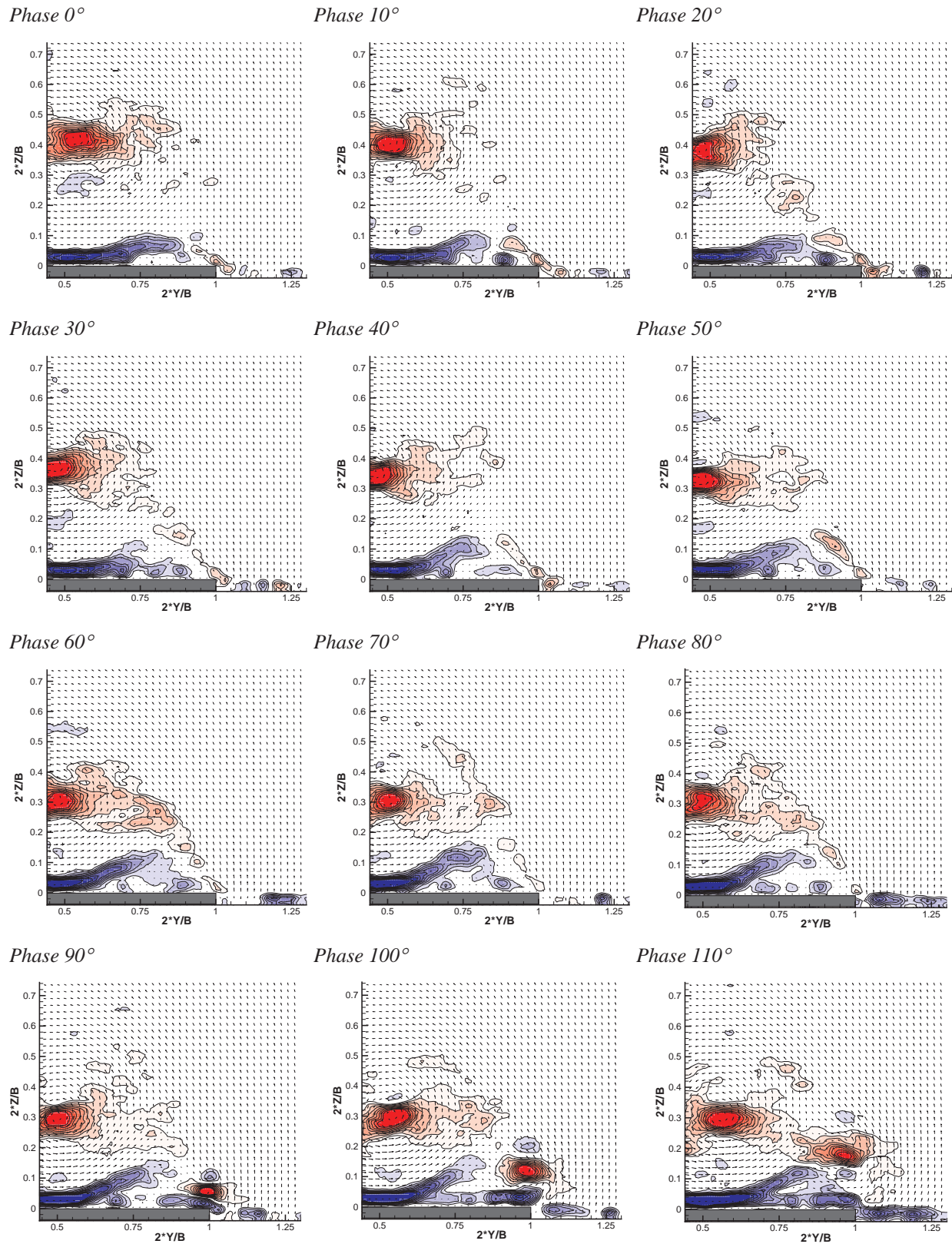


Figure 6a. Vorticity at different instants of time during one forcing cycle. $F^+ = 1.75$, $X/C = 0.4$, field of view perpendicular to wing. For contour legend see Figure 3.

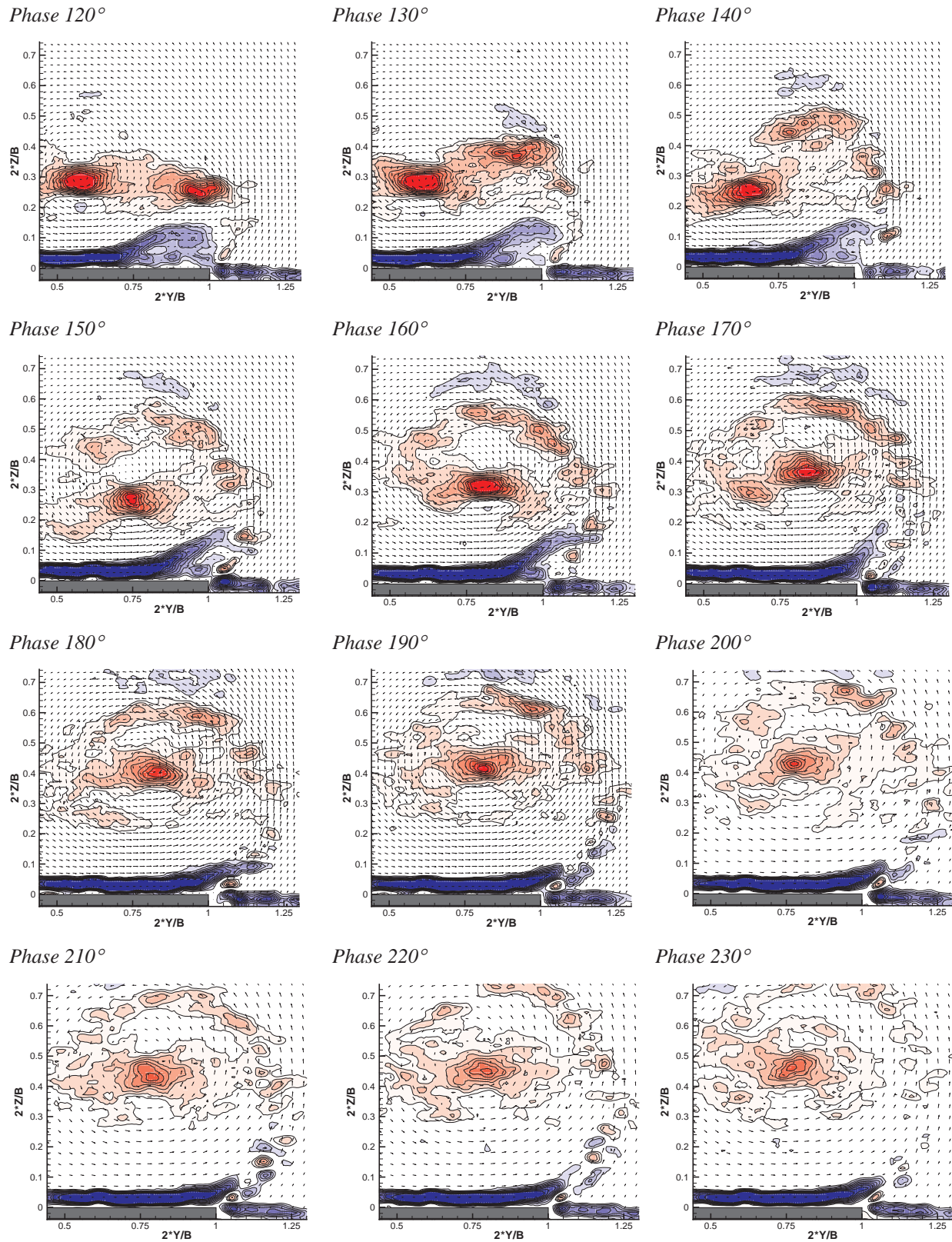


Figure 6b. Vorticity at different instants of time during one forcing cycle. $F+ = 1.75$, $X/C = 0.4$, field of view perpendicular to wing. For contour legend see Figure 3.

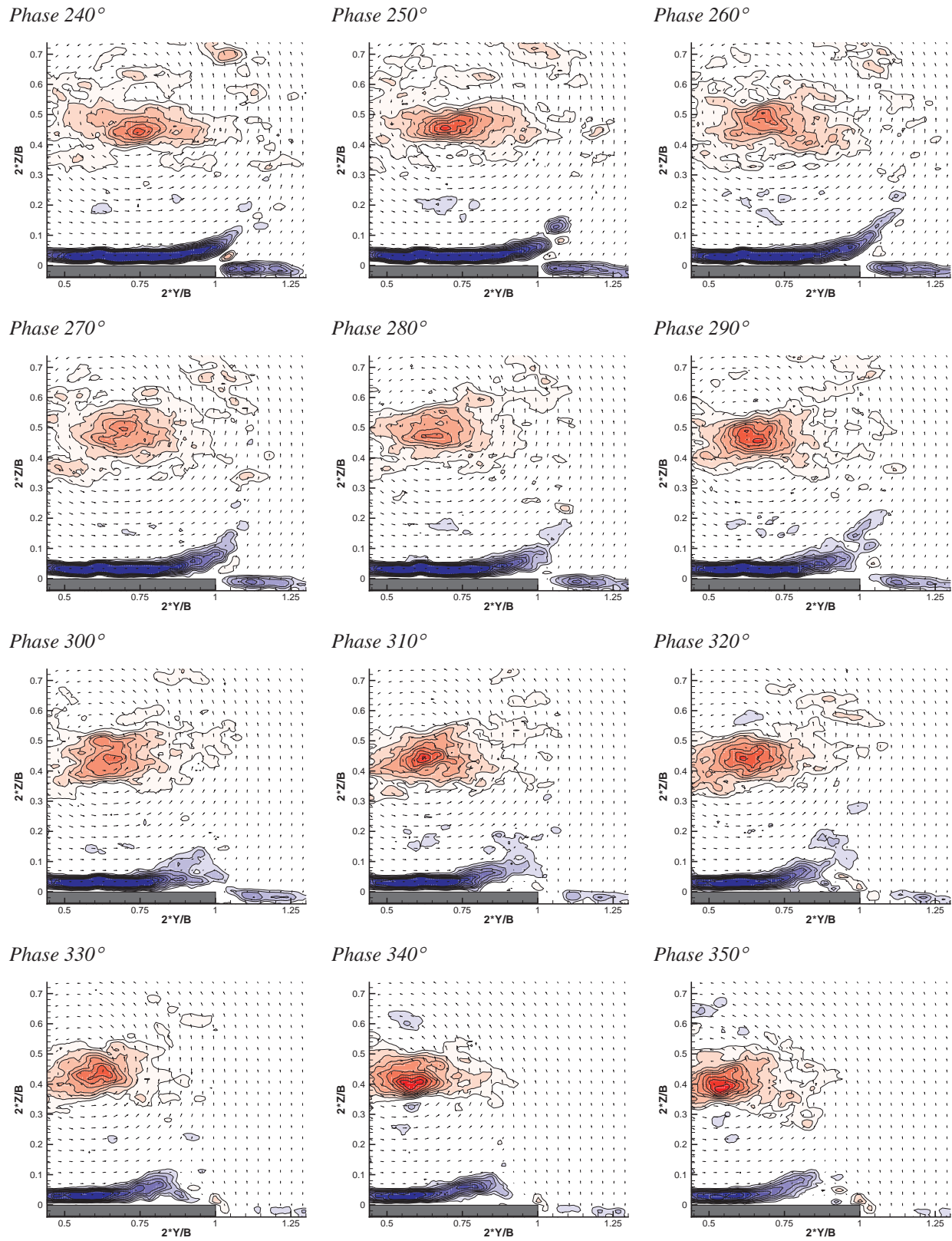


Figure 6c. Vorticity at different instants of time during one forcing cycle. $F+ = 1.75$, $X/C = 0.4$, field of view perpendicular to wing. For contour legend see Figure 3.

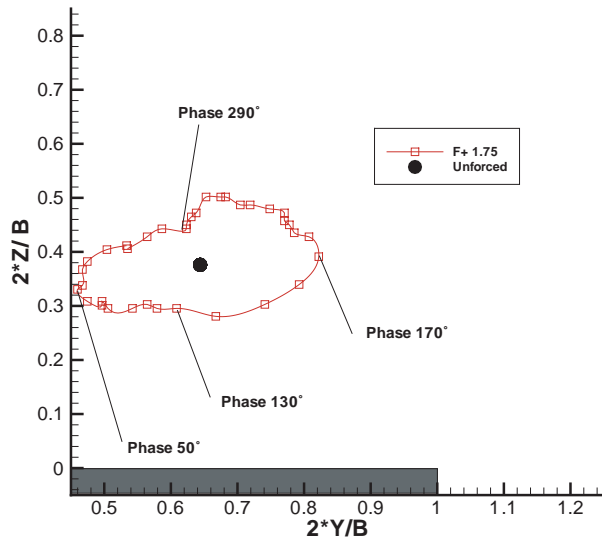


Figure 7. Location of main vortex center during the forcing cycle. $X/C = 0.4$, phase averaged data over 10 forcing cycles, field of view perpendicular to wing surface.

imum of 175% of the unforced strength. The shear layer vortex circulation peaks at 10 times of the unforced intensity at 160° in the forcing cycle, and back to near zero on the suction portion of the cycle. This circulation is merged with the main vortex, whose circulation fluctuates substantially over the course of the forcing cycle. Interestingly, the average circulation in the main vortex through one cycle does not substantially deviate from the unforced case. This indicates that the forcing does not substantially alter the average strength of the primary vortex as was previously thought.

Figure 6 a – c illustrate the PIV results for the

forced case over the entire blowing and suction cycle, starting at the beginning of the blowing cycle (0°), through the peak of the blowing phase (90°), and continuing to the 180° point, where actuator fluid ejection has stopped and begins to reverse. Sequential plots are in 10° phase increments. Note that near the 90° point, the high vorticity region near the leading edge begins to grow and starts to migrate away from the leading edge and laterally toward the wing centerline. This train of vortical flow continues as time proceeds, until a continuous “train” of vorticity feeds from the leading edge to the vortex center, occurring near 160° . At the same time the main vortex travels outboard due to induced velocities from the vortex forming in the shear layer. The entire shear layer circulation reaches a peak value that is more than twice the circulation of the unforced main vortex before it starts to merge with the main vortex. Next to the wing surface an area of negative vorticity (rotating clockwise) can be observed. During the blowing part of the forcing cycle this area of negative vorticity, which ends and lifts off the wing surface at $2*Y/B = 0.75$ in the unforced case, gets elongated until it reaches the leading edge at 180° phase. It then starts to retract again to the point where it lifts off the wing surface around $2Y/B=0.65$ at a phase of 0° . The magnitude of the circulation contained in this area of negative vorticity (not presented) reaches a maximum at about 180° phase and a minimum near 0° phase, thus oscillating in synchronization with the lift-off point.

While the forcing greatly animates the otherwise stationary main vortex, no significant changes in the circulation averaged over one forcing cycle of either the main vortex or the secondary vortex next to the wing surface could be observed. Thus there is no indication why forcing should be delaying vortex breakdown based on

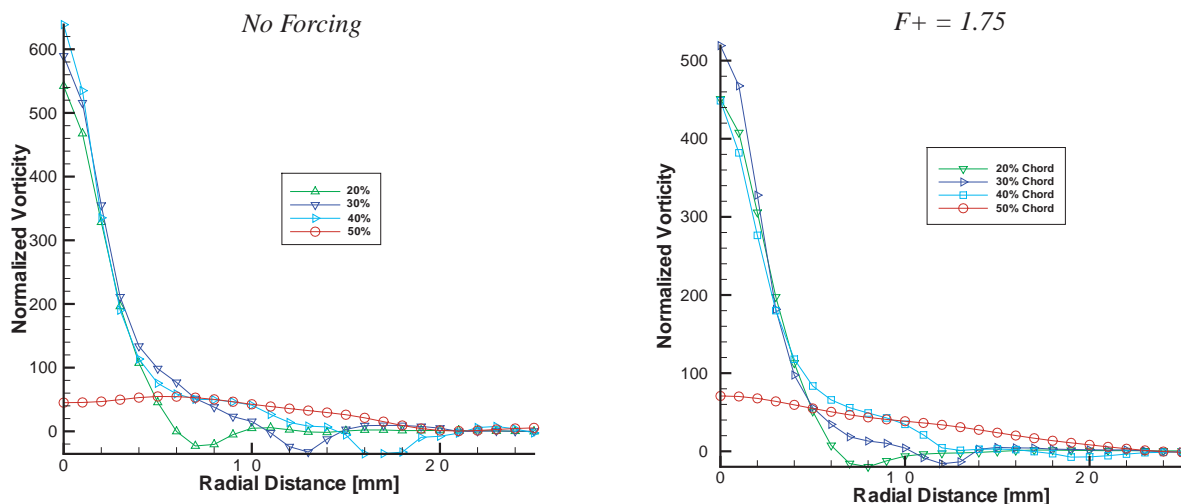


Figure 8. Vorticity Profiles of Main Vortex with and without forcing at various chord locations. Data averaged in phase and azimuthal direction. Radial distance is referenced to the instantaneous center of the vortex core.

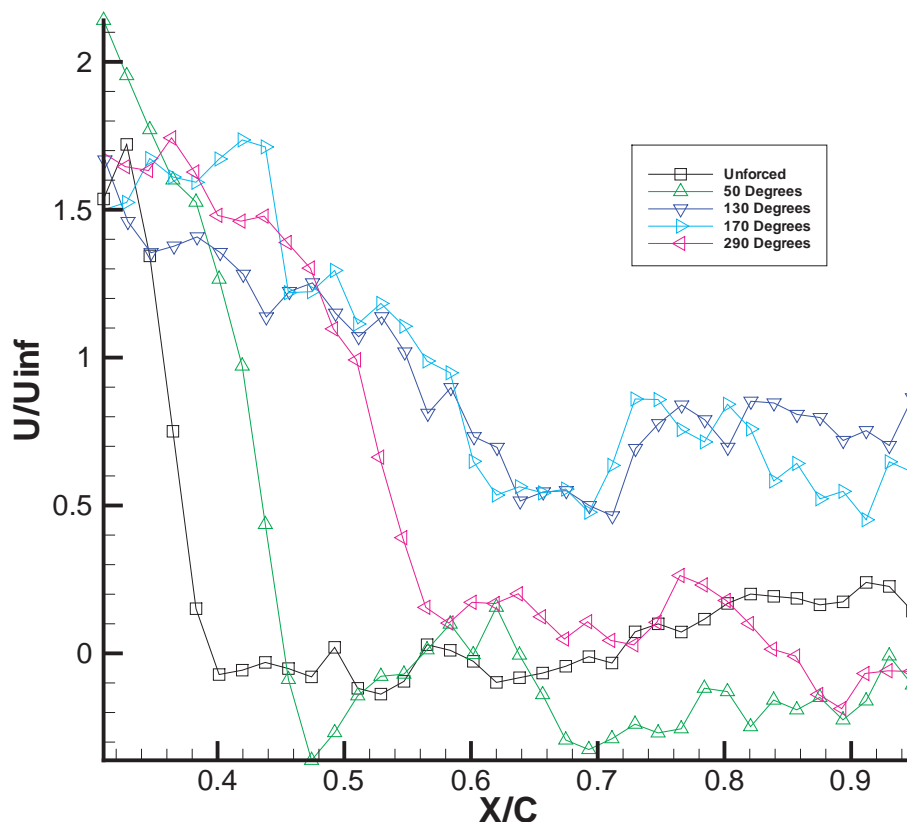


Figure 9. Axial velocity development along the vortex core. For core locations see Figure 5.

streamwise vorticity measurements.

During the suction cycle no vorticity is generated in the shear layer, most likely due to choking of the blowing and suction slot due to flow separation at the slot exit. This choking, along with some unavoidable air trapped in the blowing and suction system that adds compressibility, makes the suction portion of the forcing cycle much less efficient in forcing the shear layer than the blowing portion. During the suction cycle the main vortex travels back inboard and towards the wing surface to its starting position, while gaining in strength by absorbing the circulation of the shear layer vortex.

Using the vorticity maximum as the criterion to determine the vortex center proved highly unreliable. Especially in flow situations where there is more than one vortex present in the flow, or the vortex is highly asymmetric, it was found that location of the peak in vorticity did not coincide with the center of rotation of the flow. Therefore, the location of the main vortex was determined by tracking the minimum magnitude of the velocity in the flow field as the center of rotation. The location of this main vortex center throughout a forcing cycle is shown in Figure 7. This position information was then used to coordinate transform the PIV data from its Cartesian coordinate system to a vortex center based cylindrical coordinate system, using a second order spatial data interpo-

lation. The resulting vorticity profiles were then averaged in the azimuthal direction and, for the forced data, ensemble averaged over the 36 forcing phase angles measured. These averaged vorticity profiles are shown in Figure 8. It can be seen that the peak vorticity drops by almost a factor of ten between the downstream locations $X/C = 0.4$ and $X/C = 0.5$. This indicates breakdown of the main vortex, since at 50% chord and beyond there is no streamwise vorticity present that would qualify as a vortex, independent of the axial velocity.

The same finding is also illustrated in the vorticity contour plots, Figure 11 for the unforced case and Figure 12 for the forced case. Breakdown occurs alike for the forced and the unforced flow field, within 10% of chord resolution. In fact, there is little difference in the vorticity profiles in the forced and unforced cases downstream of vortex breakdown. Surprisingly, peak vorticity is even slightly reduced in the forced case. While the unforced findings are in good agreement with both literature and previous research at the Academy, the forced data contradicts previous findings by Guy et al who reported a downstream shift of the breakdown location by as much as 35% chord in the forced case. Their observations were based on dye flow visualization, and untriggered, time averaged laser Doppler velocimetry data. Since the position of the main vortex varies throughout the forcing cycle, non-trig-

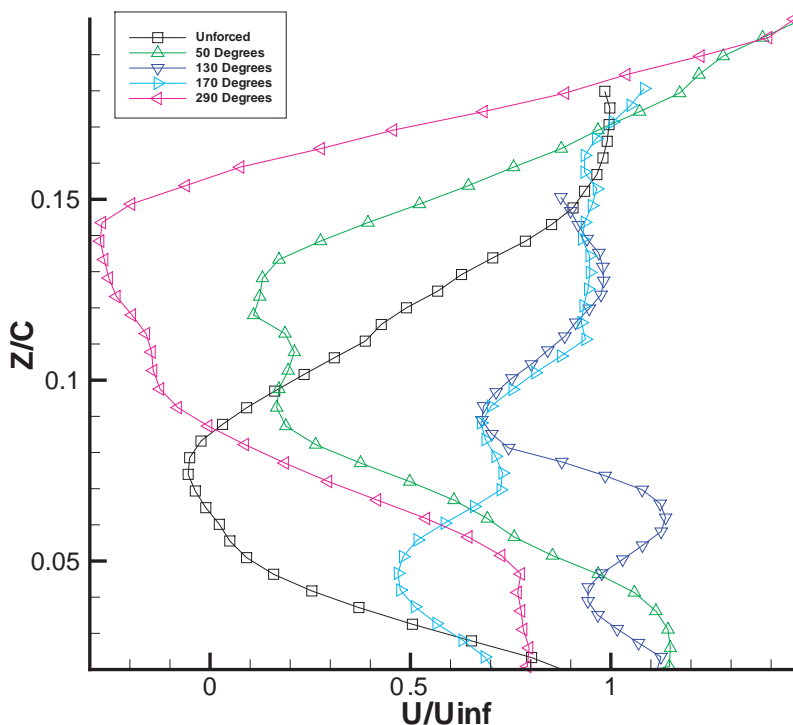


Figure 10. Axial Velocity Profiles at $X/C = 0.6$.

gered time averaging of the streamwise velocity data will yield deceptively high averages. This is because the actual wake of the broken down vortex (with small or reverse flow velocity) is only present at the measurement location for a short period throughout the forcing cycle. At all other times, the velocity outside the wake caused by the vortex breakdown will be measured. This increases the time average and wrongly indicates the presence of a coherent vortex. The flow visualization experiment was repeated by the first author of this paper, and it was found that the flow visualization shows a highly unsteady flow field where the apparent vortex breakdown location fluctuates greatly in the streamwise direction throughout the forcing cycle. Any direct breakdown location observation is therefore based on “visual averaging” and may therefore be considered suspect. Additionally, due to the unsteadiness of the flow, streakline effects may falsify the results of the observations. It is worth mentioning that the diameter of the vortex remains constant in absolute numbers until breakdown, i.e. the vortex diameter does not increase along the chord.

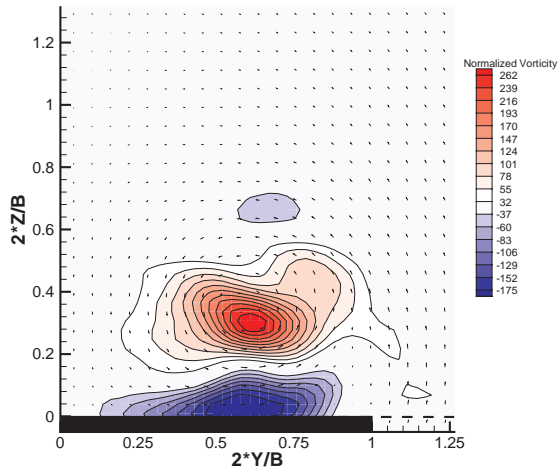
Using the vortex travel information shown in Figure 7, the measurement plane was next aligned normal to the wing at three different prominent spanwise locations within the forcing cycle: $2*Y/B = 0.45, 0.65$ and 0.8 . While $2*Y/B = 0.65$ is the spanwise location of the vortex core in the unforced case, the forced flow main vortex lines up with this location at 130° and 290° phase. $2*Y/B = 0.45$ is the most inboard position the main vor-

tex reaches, at a phase of 50° . The most outboard location is $2*Y/B = 0.8$, reached at a phase of 170° in the forcing cycle.

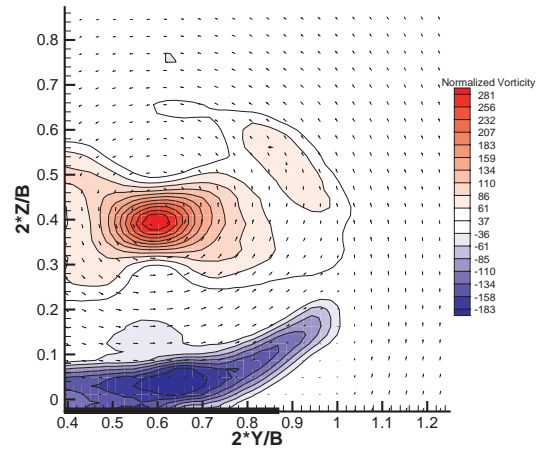
The velocity along the vortex core shown in Figure 9 indicates that for the unforced case a stagnant or slightly reversed flow develops around $X/C = 0.4$. This coincides with the location at which the vorticity in the unforced flow drops, between $X/C = 0.4$ and $X/C = 0.5$. For the forced flow, however, the location of a drop in axial velocity is dependent on the phase within the forcing cycle. For two of the phase angles investigated, 130° and 170° , no stagnant flow can be observed over the entire wing. At these phase angles, the shear layer vortex generated by the forcing is present in the flow. In the absence of the shear layer vortex, at phase angles of 50° and 290° , the forced flow does show a significant drop in axial velocity, at locations of $X/C = 0.45$ and 0.55 , respectively. One possible explanation for this behavior is that the shear layer vortex entrains fluid with high axial momentum from outside the wake left from the main vortex breakdown and thus increases the axial velocity. This would explain the decreased surface pressure found by Guy et Al extending well downstream of their observed vortex breakdown location of $X/C = 0.75$.

The wing normal velocity profiles shown in Figure 10 indicate that at $X/C=0.60$ the axial velocity near the wing surface is higher even for phase angles (50° and 290°) in which a large decrease in axial velocity can be found upstream of this location. While the decrease in

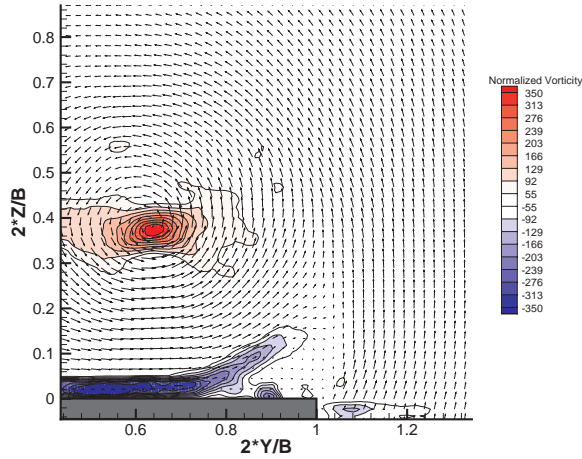
20% Chord



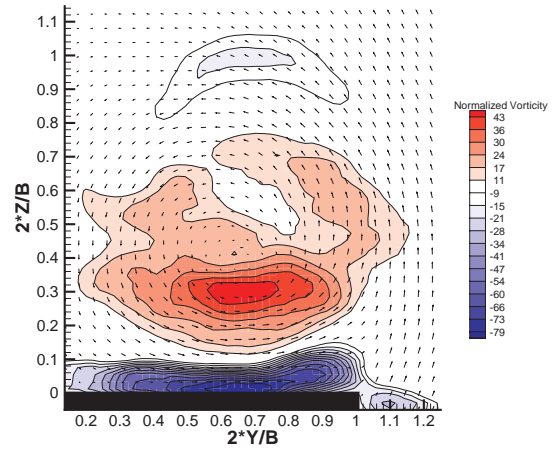
30% Chord



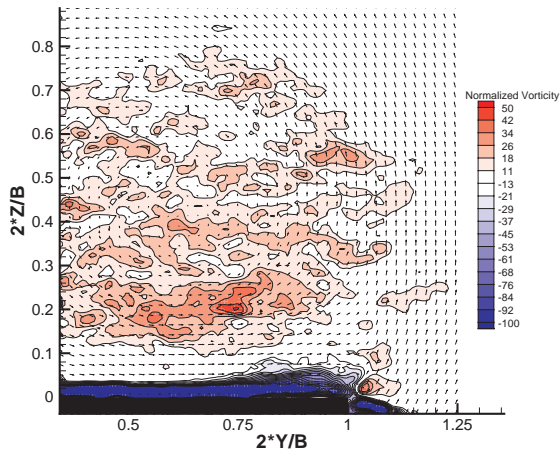
40% Chord



50% Chord



60% Chord



80% Chord

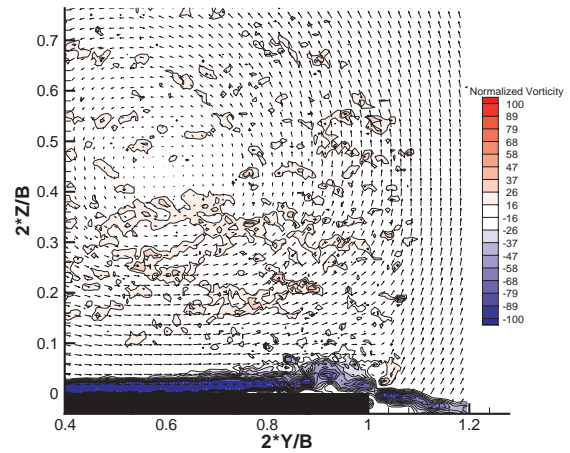
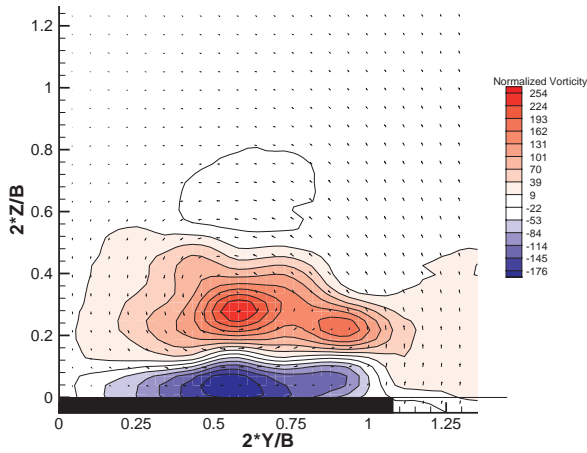
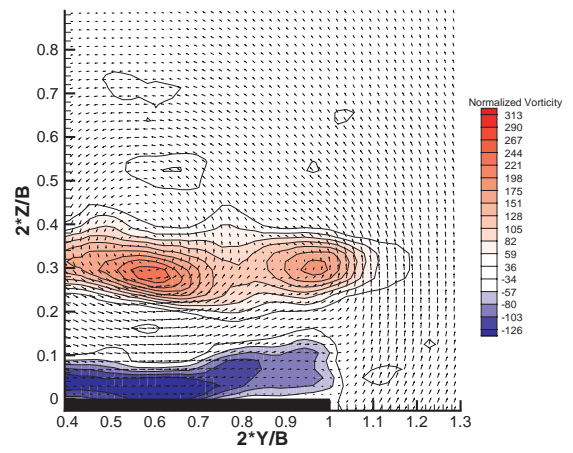


Figure 11 Downstream development of vorticity, unforced flow

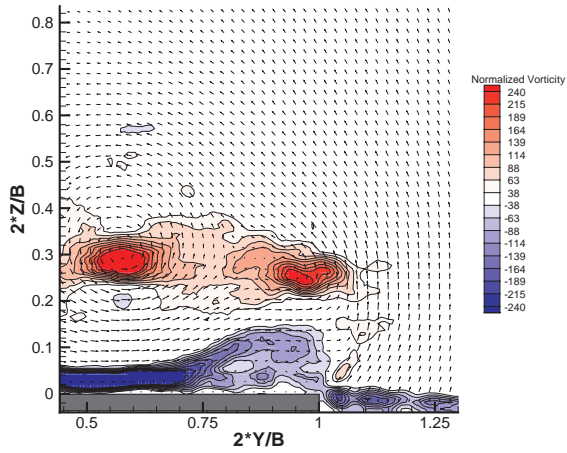
20% Chord



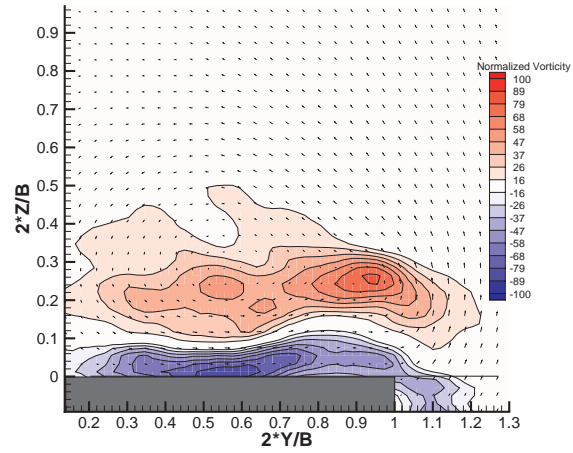
30% Chord



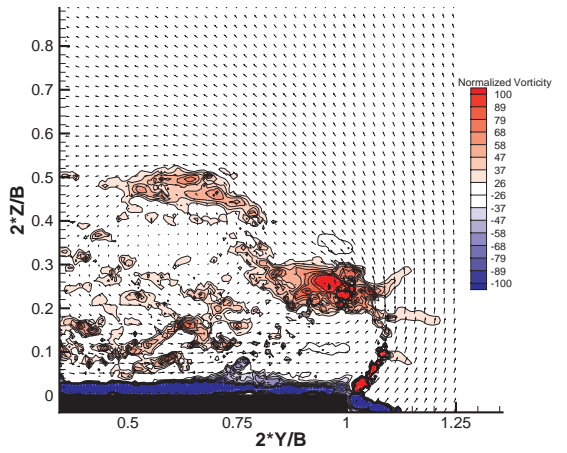
40% Chord



50% Chord



60% Chord



80% Chord

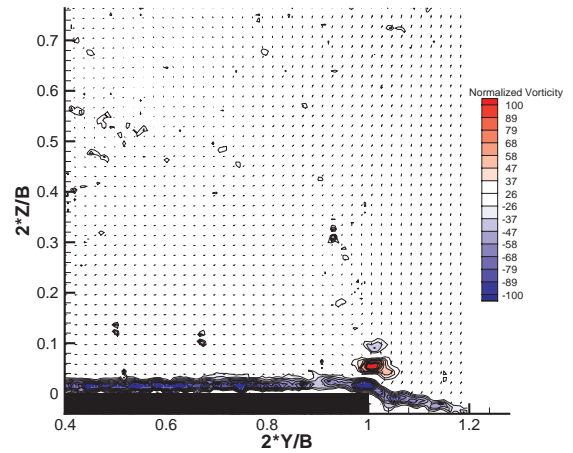


Figure 12. Downstream Development of Vorticity, $F+ = 1.75$, Phase = 120°

axial velocity is almost as large or even larger than for the unforced case, it is shifted about 0.05 chord away from the wing surface. Therefore higher velocity fluid is close to the wing, increasing the local velocity and presumably decreasing the surface pressure. This explains the total increase in normal force found in previous studies. Figure 11 and Figure 12 show the downstream development of streamwise vorticity for the unforced and forced flow fields, respectively. For the forced flow a phase of 120° in the forcing cycle was chosen, at which time the shear layer vortex has just formed and starts to travel away from the wing. It can be seen that the shear layer vortex is present along the entire leading edge of the wing, and becomes the strongest vortex in the flow downstream of vortex breakdown. Vortex breakdown of the main vortex occurs independently of the forcing between 40% and 50% chord.

Conclusions

The flow over a 70° delta wing at a chord Reynolds number of 25,000 and an angle of attack of 35° was investigated in water tunnel experiments. The flow was forced using sinusoidal blowing and suction along the entire leading edge at a non-dimensional frequency of $F^+ = 1.75$. It was found that periodic blowing and suction does not delay vortex breakdown as previously reported by Guy, Morrow and McLaughlin. The vortex breakdown took place between $X/C = 0.4$ and 0.5 for both the forced and unforced case, as evidenced by a drop in vorticity by almost an order of magnitude. For the unforced flow the location of the drop in streamwise vorticity was found to coincide with a drop in axial velocity. For the forced flow the location where the axial velocity dropped abruptly was fluctuating throughout the forcing cycle between $X/C = 0.45$ and downstream of the trailing edge. Thus a drop in axial velocity cannot be used to determine vortex breakdown for the forced flow. The forcing resulted in an overall increase in axial velocity in the vortex core near the wing surface, especially beyond vortex breakdown. This may explain the increase in normal force reported in previous studies.

Outlook

Since forcing does not appear to improve the flow upstream of vortex breakdown, future experiments are planned to investigate the effect of forcing along parts of the leading edge only instead of the entire leading edge. Also, forcing methods that may improve the location of vortex breakdown by altering the shape of the vortex core from straight to curved by using spatially modulated forcing upstream of the natural vortex breakdown location are being considered.

References

1. Guy, Y., Morrow, J. A., McLaughlin, T. E., "Control of Vortex Breakdown on a Delta Wing by Periodic Blowing and Suction", AIAA Paper 99-0132, 1999.
2. Guy, Y., Morrow, J. A., McLaughlin, T. E., and Wygnanski, I., "Pressure Measurements and Flow Field Visualization on a Delta Wing with Periodic Blowing and Suction", AIAA Paper 99-4178, 1999.
3. Greenblatt, D. and Wygnanski, I., "Dynamic Stall Control by Oscillatory Forcing", AIAA Paper 98-0676, 1998.
4. Nishri, B., "On the Dominant Mechanisms Governing Active Control of Separation", Ph.D. Thesis, Tel-Aviv University, Israel
5. Nishri, B. and Wygnanski, I., "On the Flow Separation and its Control", Computational Methods in Applied Science, 1996.
6. Seifert, A., Darabi, A. and Wygnanski, I., "Delay of Airfoil Stall by Periodic Excitation", AIAA Journal of Aircraft, Vol. 33, No. 4, 1996.
7. Nave, T., "The Effect of Sweep on Separation Control over an Airfoil", M.Sc. Thesis, Tel-Aviv University, Israel, 1997.
8. Seifert, A., Darabi, A. and Wygnanski, I., "The Effects of Forced Oscillations on the Performance of Airfoils", AIAA Paper 93-3264, 1993.
9. Wygnanski, I. and Seifert, A., "The Control of Separation by Periodic Oscillations", AIAA Paper 94-2608, 1994.
10. Guy, Y., Morrow, J. A., McLaughlin, T. E., and Wygnanski, I., "Velocity Measurements on a Delta Wing with Periodic Blowing and Suction", AIAA Paper 00-0550, 2000.
11. Guy, Y., Morton, S.A., Morrow, J. A., "Numerical Investigation of the Flow Field on a Delta Wing with Periodic Blowing and Suction", AIAA 2000-2321, 2000.